Early Evolution of the Hunga-Tonga Stratospheric Aerosol Plume observed by Lidar at La Réunion (21°S, 55°E)

Alexandre Baron[1], P Chazette[2], S Khaykin[3], G Payen[4], N Marquestaut[4], N Bègue[1], and V Duflot[1]

[1]Laboratoire de l'Atmosphère et des Cyclones (LACy), UMR 8105 CNRS, Université de la Réunion, Météo-France, 97400 Saint-Denis de La Réunion, France
[2]Université Paris-Saclay -CEA -CNRS -UVSQ
[3]Sorbonne Université -UVSQ -CNRS
[4]Observatoire des Sciences de l'Univers de La Réunion (OSU-Réunion)

November 23, 2022

Abstract

The highly-explosive eruption of the Hunga-Tonga Hunga Ha'apai volcano (HTHH), that occurred on 15 Jan. in the South Pacific, was associated with a powerful blast that injected gases, steam and aerosols to unprecedentedly high altitudes. Here we present unique observations of the young volcanic aerosol plumes by ground-based lidars at La Reunion island (21°S, 55°E), located directly downwind of the eruption. Two lidars, operating at 355 nm and 532 nm, sampled the overflying plume every nights from 19 Jan. until 28 Jan. We assess both the vertical structure and the optical properties. A wide plume altitude range from 36 km down to 18 km has been highlighted along time, with heterogeneous aerosol optical depth that reached 0.84 at 532 nm and Angström exponents from-0.8 to 1.2. Such temporal evolution is related to both the injection heights of the volcanic material and the stratospheric dynamic and chemistry.

Early Evolution of the Hunga-Tonga Stratospheric Aerosol Plume observed by Lidar at La Réunion (21°S, 55°E)

A. Baron[1], P.Chazette[2], S.Khaykin[3], G. Payen[4], N. Marquestaut[4], N. Bègue[1] and V. Duflot[1]

[1]Laboratoire de l'Atmosphère et des Cyclones (LACy), UMR 8105 CNRS, Université de la Réunion, Météo-France, 97400 Saint-Denis de La Réunion, France.

[2]Laboratoire des Sciences du Climat et de l'Environnement, LSCE-IPSL, UMR 8212, Université Paris-Saclay - CEA - CNRS - UVSQ, Gif-sur-Yvette, France.

[3]Laboratoire Atmosphère Milieux Observations Spatiales, LATMOS-IPSL, UMR 8190, Sorbonne Université - UVSQ - CNRS, Paris, France.

[4]Observatoire des Sciences de l'Univers de La Réunion (OSU-Réunion), UAR 3365, Université de la Réunion, CNRS, Météo-France, 97400 Saint-Denis de La Réunion, France.

Corresponding author: Alexandre Baron (alexandre.baron@univ-reunion.fr)

Key Points:

- Unprecedented altitude of a plume of volcanic aerosol observed by a ground-based lidar
- Unprecedented aerosol optical depth and extinction values observed in the stratosphere
- Evidence of rapid evolution in structure and optical properties of fresh volcanic aerosols in the stratosphere

Abstract

The highly-explosive eruption of the Hunga-Tonga Hunha Ha'apai volcano (HTHH), that occurred on 15 Jan. in the South Pacific, was associated with a powerful blast that injected gases, steam and aerosols to unprecedentedly high altitudes. Here we present unique observations of the young volcanic aerosol plumes by ground-based lidars at La Reunion island (21°S, 55°E), located directly downwind of the eruption. Two lidars, operating at 355 nm and 532 nm, sampled the overflying plume every nights from 19 Jan. until 28 Jan. We assess both the vertical structure and the optical properties. A wide plume altitude range from 36 km down to 18 km has been highlighted along time, with heterogeneous aerosol optical depth that reached 0.84 at 532 nm and Angström exponents from -0.8 to 1.2. Such temporal evolution is related to both the injection heights of the volcanic material and the stratospheric dynamic and chemistry.

Plain Language Summary

Stratospheric aerosols have the potential to significantly impact the climate at global scale. The backscatter of solar irradiance to space by these particles unbalance the Earth radiative budget following massive material injections in the stratosphere. This process can induce important surface temperatures decrease as previousy shown following past major volcanic eruptions. In January 2022, the Hunga-Tonga volcano erupted in the southern Pacific (20.5°S, 175.4°W). The caracteristics of this remarkable Plinian eruption allow to deepen our understanding of key processes associated with a massive injection of both gases and particles into the stratosphere. Based on laser remote-sensing observations of the Hunga-Tonga aerosol plume in the mid-stratosphere, the structural and optical properties of the volcanic plume were assessed during its passage over Reunion Island (21°S, 55°E). Our results show a significant and unprecedented evolution of the optical properties of aerosols trapped in the volcanic plume as a function of its altitude. These are original and essential observations to improve our understanding of the radiation balance in the stratosphere and to model it in global climate models.

1 Introduction

Our knowledge of injections of aerosols in the stratosphere and their feedbacks on climate comes from observations of previous massive injections triggered by historic volcanic eruptions (Kremser et al., 2016; Robock, 2015) that occurred periodically (Delmas et al., 1992; Tejedor et al., 2021) and more recently following extreme wildfires, that are likely to increase with climate change (Di Virgilio et al., 2019; Peterson et al., 2018), generating pyroconvection processes able to inject carbon-rich aerosols into the lower stratosphere (Khaykin et al., 2020; Yu et al., 2019). On the volcanic side, the most recent climate impacting event occurred in 1991 during the eruption of Mount Pinatubo (e.g. Hansen et al., 1992). This event is abundantly documented throught observational and modeling studies (Boville et al., 1991; Chazette et al., 1995; DeFoor et al., 1992; Gobbi et al., 1992; Graft et al., 1993; Grant et al., 1992; McCormick et al., 1995; Minnis et al., 1993). These studies showed an average global cooling of 0.5-0.7°C in the year following the eruption due to sulphate aerosols associated with the gaseous precursor SO_2 (sulphur dioxide). A specific study has also shown the influence of these particles in the thermal infrared spectrum and highlighted their detectability from Earth observing satellites (Pierangelo et al., 2004). However, it is still difficult to quantitavely assess the amount of SO_2 that has been injected to produce the observed cooling of Earth in the following years (Dhomse et al., 2020; Guo et al., 2004; M. P. McCormick & Veiga, 1992). The injected mass of SO_2 is known to within a factor of two that can

be attributed to both parametrization of involved physical processes and uncertainties on observations (Bluth et al., 1992; Dhomse et al., 2020).

In order to bring the models studying the impact of stratospheric aerosols on climate to a consensus, it is up to the experimenters to propose reliable observations to constrain the parameterisation of processes implemented in climate models. This is challengeing since we denote only three major eruptions in the 20th century: the Mount Agung, El Chichon and the Mount Pinatubo (J. K. Angell, 1993; Dhomse et al., 2020). All three were characterized by a Volcanic Explosivity Index (VEI) superior or equal to 5 and were followed by a significant decrease of the tropospheric and surface temperatures (James K. Angell, 2000; Robock & Mao, 1995).

The eruption of the Hunga-Tonga Hunha Ha'apai volcano (HTHH) that occurred in the South Pacific (20.5°S, 175.4°W) is currently extensively observed since its eruption on 15 Jan 2022. Its shallow underwater caldera has contributed to an extremely powerful blast triggering the so called phreato-plinian eruption (Yuen et al., 2022). The blast, estimated to range between 100-200 MT of TNT equivalent (Vergoz et al., 2022), was detected in Alsaka, more than 9000 km away (Yuen et al., 2022). It generated a pressure wave measured all around the globe (Amores et al., 2022) and a worldwide Tsunami (Carvajal et al., 2022). On the atmospheric side, the disturbance generated by the expulsion of water, ash and gas has pierced the tropopause and even the stratopause according to stereoscopic measurements allowed by two geostationary satellites (Carr et al., 2022; Millán et al., 2022). While the climate impact of HTHH eruption is yet to be evaluated, its VEI of almost 6 and the stratospheric perturbation induced can certainly place this event along the very large eruptions mentioned for the 20th century (Khaykin et al., Submitted; Poli & Shapiro, 2022).

Given the westward zonal wind flow in the stratosphere, the volcanic material injected above the tropopose rapidly headed toward the Indian Ocean, stably centred around the 20°S latitude belt. Directly in the path of the plume, 12,800 km away from the Tonga archipelago, the French oversea region of La Réunion island (21°S, 55°E) stands in the southwest of the Indian Ocean as its highest peak. This island hosts the Atmospheric Physics Observatory of La Réunion (OPAR). The observations performed from OPAR sampled the early evolution of the aerosol plume just four days after the eruption, while it is still weakly dispersed according to satellite observations (Legras et al., 2022). Such early observations have not been possible for past remarkable events of the 20th century: for HTHH this dataset will help to understand the key processes occurring in the fresh volcanic stratospheric plume (VSP).

Two lidars have been operated at La Réunion for stratospheric aerosol measurements at 355 nm and 532 nm every night during the first overpass of the VSP, from its arrival on 19 Jan until 28 Jan. This continuous sampling of the stratosphere allows to asses both the vertical structures and the optical properties of the VSP as it progress zonaly. The synergy between the two lidars at different wavelengths gives the opportunity to retrieve the aerosol extinction coefficients and the lidar ratios, and their spectral dependencies between 355 and 532 nm. Such data made it possible to constrain Mie modeling to draw some conclusions on the evolution of the particle size during the volcanic plume passage.

In the following, the technical aspects inherent to lidar systems and inversion protocol of the aerosol optical properties are shortly presented in Section 2. We then present and discuss the plume vertical structure in Section 3 as it was observed above La Réunion. The evolution of the optical properties of the different observed aerosol layers are then displayed in Section 4 before the discussion that conclude the paper.

2 Instruments and Methods

2.1 OPAR Lidars

OPAR is a permanent station located in the French volcanic island of La Réunion. It is dedicated to long term atmospheric observations: dynamic and physico-chemistry of the low and middle atmosphere in the Southern Hemisphere. It is a French Instrumented Site labelleded by Institut National des Sciences de l'Univers (INSU) of CNRS. The Maïdo Observatory (Baray et al., 2013) is a facility located on the Maïdo mount (2160 m above the mean sea level - AMSL, lee side on the tropical island). Its situation allows particularly favorable observing conditions for nighttime lidar measurements. Aerosol observations are then performed routinely at Maïdo Observatory since 2013 thanks to two lidar systems: the LiO_3T and the Li1200. The Li1200 system is dedicated to the measurement of water vapor in the troposphere and of aerosols in the troposphere and stratosphere (Dionisi et al., 2015; Vérèmes et al., 2019). The Li1200 is based on the two 30 Hz pulsed Nd:YAG lasers emitting at 355 nm with an energy per pulse equivalent to 800 mJ after beams-recombination. The reception system composed by a 1200 mm parabolic mirror (7.2 m effective focal length) and the Licel electronics allow to record profiles every 1 min with a vertical resolution downgraded to 15 m. The LiO_3T system is dedicated to the measurement of ozone in the troposphere and of aerosols in the troposphere and stratosphere (Duflot et al., 2017). The aerosol component of the LiO_3T is based on a Nd:YAG laser emitting 532 nm pulses of 250 mJ at a frequency of 30 Hz, and a reception system composed by a 500 mm parabolic mirror (1.5 m focal length) and an optical fiber (1 mm diameter) at its focus point to collect the backscattered light, which is detected by a photomultiplier. The profiles are recorded every 2 min with a vertical resolution of 7.5 m.

For both lidar systems, the altitude range of interest is above the overlap factor, so the latter has no impact on the observations in the stratosphere. For the two lidars, the profiles are averaged over 5 minutes and 50 m before the retrieval of aerosol optical properties. This allows both homogeneisations of the two datasets and an enhancement of the signal to noise ratio (SNR).

2.2 Retrieval of Optical Properties

Aerosol layers transported in the stratosphere are often sandwiched between clean aerosol-free air parcels, generally stated as a molecular background, whose optical behavior follows the Rayleigh scattering framework. Using the Rayleigh slope method (RSM) as used by Chazette et al. (1995), it is then quite straitforward to retrieve the aerosol optical depth (AOD) of the volcanic aerosol in the stratospheric layers (VASL). This AOD derived with RSM is then used as an input for an iterative Klett inversion method (Klett, 1985) as proposed by Chazette et al. (2012) to retrieve simultaneously the vertical profile of aerosol extinction coefficient (AEC) and the lidar ratio (LR). The latter, which is namely the ratio of the aerosol extinction to backscatter coefficients, provides indications on some microphysical properties of the observed aerosols and is often used to classify aerosol types (Müller et al., 2007; Chazette et al., 2016).

3 Structures of the Stratospheric Aerosol Plumes

The sequence of measurements is presented in Figure 1. It shows the AEC of the different aerosol layers that overflew La Réunion during the second half of January 2022 (Fig.1a). Fig.1b shows the scattering ratio (SR), which is the ratio of the total volume basckatter and the volume molecular backscatter coefficients. This parameter is convenient when it comes to appreciate the order of magnitude of the aerosol perturbation, a value of 1 corresponds to clear skies and greater than 1 to

the presence of aerosols. Fig.1c shows the wind profile as reanalyzed by the European Center for Medium-Range Weather Forecast (ECMWF) through the ERA5 product at 0.25° of resolution (Hersbach et al., 2020). We used a inverse-distance weighted average from the nine grid points surrounding the Maïdo mount to have a collocated profiles and averaged theseones during the period of measurement. The concomitant local radiosoundings and there mean are also plotted.

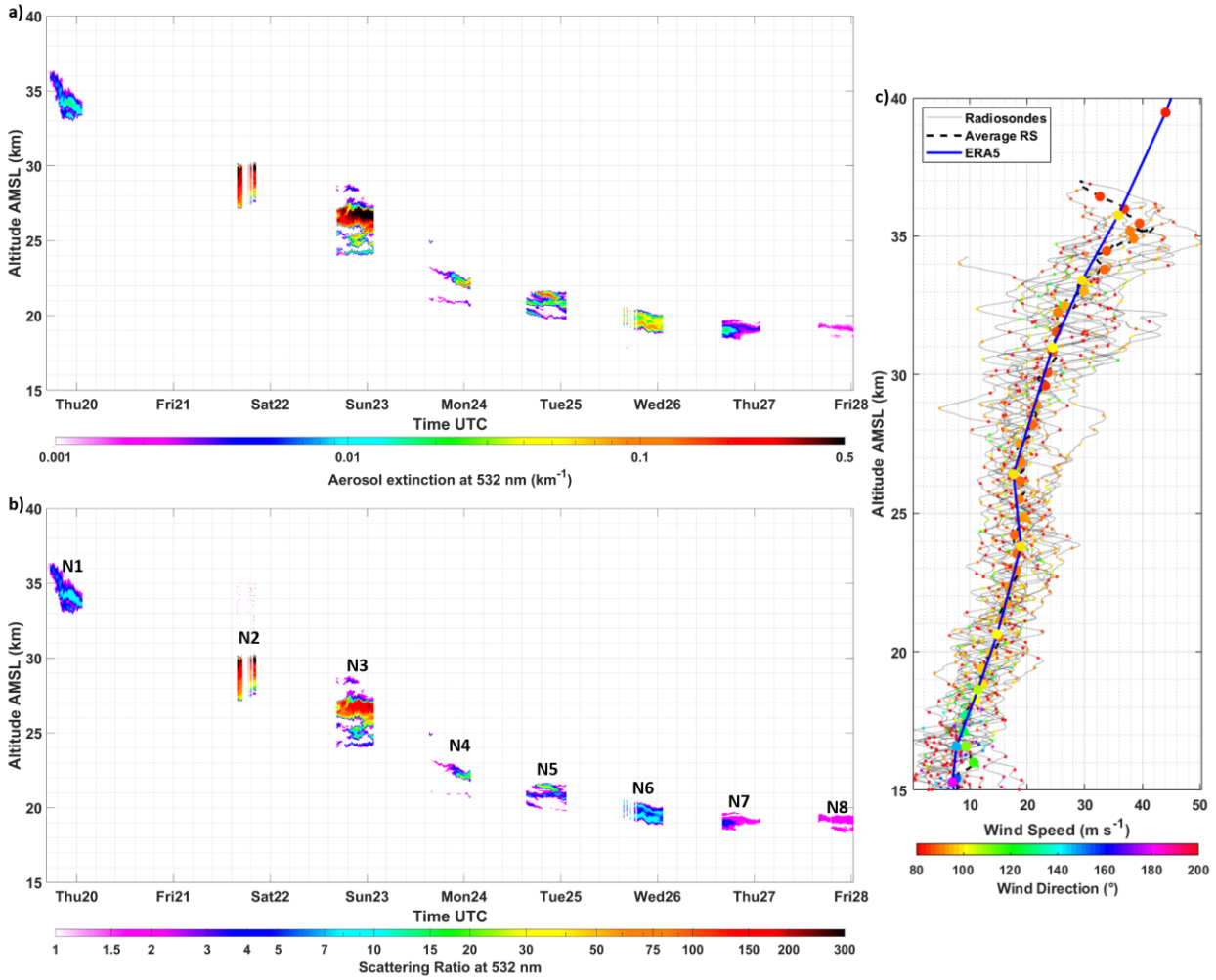

Figure 1: Overview of the stratospheric aerosol perturbation overflying La Réunion. The time-height cross-sections of aerosol extinction coefficient (a) and scattering ratio (b) at 532 nm derived from LiO_3T profiles are plotted. The different Volcanic Aerosol Stratospheric Layers (VASL) are named from N1 to N8 (b) corresponding to every night of observation showing a significant aerosol burden from 19 to 28 Jan. Altitude range is restricted to the stratosphere where the plume was sampled between 17 km and 38 km Above the Mean Sea Level (AMSL). Note the logsacle of the colorbar. Wind profiles are shown (c) for each radiosonde launches during the period (pale grey lines and thick dashed line as the average), and the output of ERA5 is superimposed (thick blue line). The color in (c) informs on the direction of the wind.

One can note on Fig. 1a and 1b an inverse comma shape which is typical of early observations of volcanic plumes transported over long distances. The same shape was observed in the troposphere above Paris following the Eyjafjallajökull eruption in 2010 (Chazette et al., 2012). Even if the Hunga-Tonga eruption sequence presents several pulses (Poli & Shapiro, 2022), the event is still quite short (~20 hr). This chronology cannot be responsible for the successive delays observed for the layers at different altitudes. This shape is driven by the strong vertical gradient of zonal wind

in the stratosphere. Indeed, routine radiosonde measurements conducted at La Réunion (Fig.1c) show a peak wind speed of 15 m s^{-1} around 18-20 km AMSL, a value that triples to 40-45 m s^{-1} at the altitude of the highest observed layer (35 km AMSL). The wind profile also shows that the flow is mainly zonal in this latitude band. The initially vertical eruptive column has thus bent under the influence of the horizontal wind shear during its transport from the Tonga to La Réunion.
This high wind velocity in the mid-stratosphere also explains the precocious arrival of the layer N1 sampled during the 19-20 January night between 33 and 36 km. It made the 12,800 km journey in 108 hr at a mean cruising speed of ~33 m s^{-1}, a value that corresponds to Fig.1c suggesting an highly stable flow along the way. These particles reached an impressive altitude that, to our knowledge, was never observed before by ground-based instruments. These particularities are due to the high performances of the used lidar systems for stratospheric measurements and to the power of the phreato-plinian eruption which saw its initial atmospheric disturbance reaching 58 km AMSL (Carr et al., 2022).

4 Temporal and Vertical Evolutions of the Aerosol Optical Properties

Although N1 is optically thin (max AEC ~ 0.03 km^{-1} at 355 nm, see Figure 2) in contrast to the layers arriving afterwards (especially N2 and N3), it is still a significant aerosol load for the stratosphere knowing that the AEC background is not exceeding 10^{-4} km^{-1} at these altitudes (Vernier et al., 2011). Given its relatively low AEC, N1 was not easily observed from passive remote sensors onboard satelittes but CALIOP onboard CALIPSO (Winker et al., 2003) observed a tenuous layer between 35-40 km during its orbit between Australia and New-Zealand Jan 15 at 1500UTC (CALIOP orbit N1, 2022). According to CALIOP this VASL shows linear particle depolarization ratio around 30%. At OPAR, only the Li1200 working at 355 nm offered a sufficient SNR (> 60) to apply the RSM and assess the AEC, AOD and LR of N1 (Fig.2).

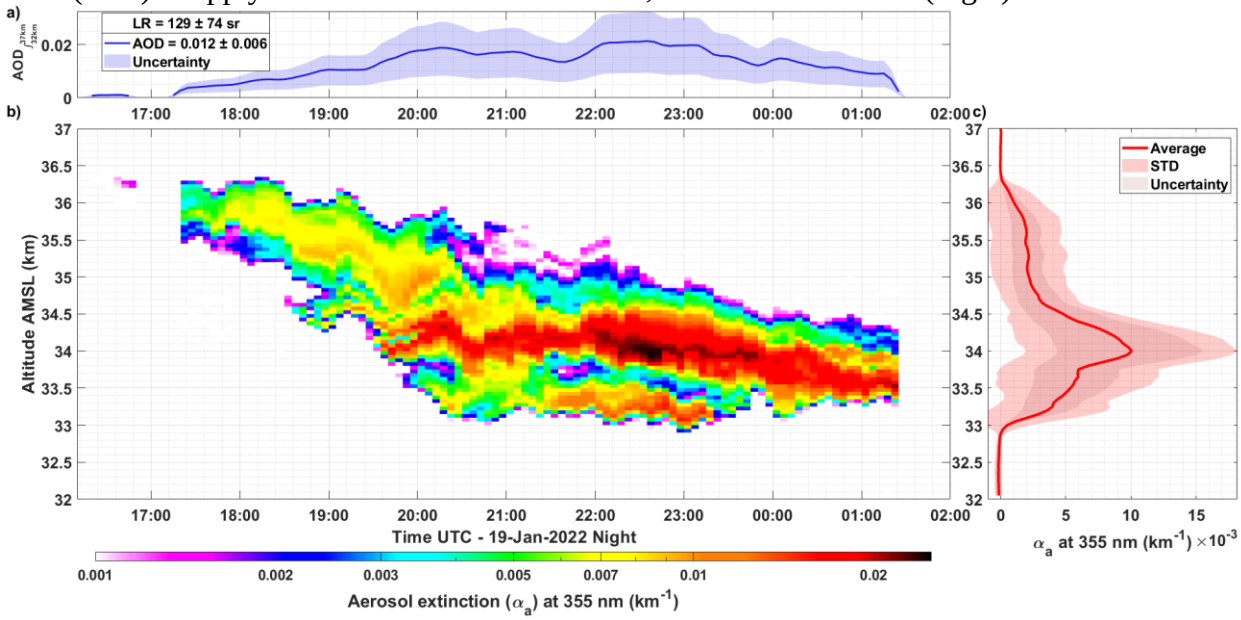

Figure 2: Evolution of the aerosol optical properties during the 19-20 Jan. night for the volcanic aerosol layer N1. The aerosol optical depth time series at 355 nm calculated between 32 and 37 km is displayed (a). The aerosol extinction coefficient (α_a) time-height cross section is plotted with a logscale colorbar (b) and the corresponding averaged profile is drawn in red (c).

We can clearly see on Fig. 2 the bulk of N1 around 34 km AMSL. The lidar-derived LR is surprisingly high (129 sr) and the associated uncertainty (74 sr) denotes the difficulty to have a trusty caracterisation of this VASL that could be composed of a aerosol mixture with a wide range of properties. A mixture of fine ash, sulfates and even marine aerosol could not be excluded given the unprecendented power of the under-water explosion. It is therefore not certain that the plume is homogeneous as a function of altitude and that a LR equivalent to the aerosol column is representative of a well identified particle type.

Two days later, N2 is located between 27 and 30 km. It is exceptionnally thick, both geometricaly (2-3 km, Fig.1ab) and optically, with maximum AOD values reaching 0.84 at 532 nm (see table 1). To our knowledge, this is unprecedently observed in the stratosphere. It doubles the former record of 0.4 measured at Mauna Loa Observatory 90 days after the Pinatubo eruption (Antuña et al., 2002). Accordingly, the peak value of SR up to 404 at 532 nm (resp. 107 at 355 nm) is really to be noted as what could be the greatest stratospheric perturbation by aerosols at this altitude since the Krakatoa (Khaykin et al., Submitted).

The following night was ideal for lidar observations. We sampled N3, another dense layer between 24 and 28 km presenting values of AEC reaching 0.41 km^{-1} at 355 nm (Table 1). Even if they share remarkable values of AEC and AOD and close LR estimates, N2 and N3 are distinct. The different timing of passage, and the layers contours argue in favor of two independent layers (Fig.1ab). This separation is also corroborated by CALIOP (Legras et al., 2022) that sampled this double layer several times between Januay 16 and 19. We can also note from these measurements that after N1 all the VASL share near zero CALIOP-derived depolarization values indicating spherical aerosol shapes (Legras et al., 2022).

N3 seems to end with the beginning of N4 appearing lower in altitude (~22 km AMSL, Fig.1ab and Table 1). N4 is a thiner filamentary layer followed the next nights by N5 to N8 which tend to be lower in altitude and finally decrease in terms of AOD. To summarize extensively the significant properties of the plume, they are detailed in the Table 1.

Table 1: Summary of the principal geometrical and optical characteristics of the plume. It is detailed following the Fig. 2b naming of the different layers and date (N1 to N8). AOD stands for Aerosol Optical Depth, AEC for Aerosol Extinction Coefficient and SR for Scattering Ratio. The value given are night averaged with associated standard deviations. The maximum is also added in parantheses as well as the atltiude where it could be found ("peak" in the altitude column). Note that for N1, N7 and N8 at 532 nm and N8 at 355 nm the measurements do not comply with the thresholds of signal to noise ratio, AOD and attenuated SR to be processed with our method. Thus only attenuated SR are provided.

Layers (Jan. Night)	Altitude Range (peak) [km]	λ [nm]	AOD (max)	AEC peak (max) [km^{-1}]	SR peak (max)	Lidar ratio [sr]	Angström exponent
N1 (19)	33 – 36 (34.1)	355	0.01 ± 0.01 (0.03)	0.01 ± 0.01 (0.03)	2.2 ± 1.0 (3.9)	129 ± 74	-
		532	-	-	5.8 ± 3.6 (12)	-	
N2 (21)	27 – 30 (29.7)	355	0.44 ± 0.10 (0.59)	0.31 ± 0.03 (0.41)	80 ± 9.0 (107)	30 ± 2	-0.8 ± 0.8
		532	0.60 ± 0.15 (0.84)	0.45 ± 0.05 (0.66)	272 ± 33 (404)	69 ± 11	
N3 (22)	24 – 28 (26.8)	355	0.31 ± 0.09 (0.43)	0.30 ± 0.09 (0.41)	45 ± 13 (61)	33 ± 6	-0.7 ± 0.9
		532	0.41 ± 0.10 (0.55)	0.43 ± 0.14 (0.63)	150 ± 50 (218)	75 ± 7	
N4 (23)	21 – 23 (22.1)	355	0.01 ± 0.01 (0.04)	0.03 ± 0.04 (0.12)	3.0 ± 3.1 (10)	29 ± 5	0.0 ± 3.5
		532	0.01 ± 0.01 (0.04)	0.03 ± 0.04 (0.13)	6.7 ± 9.0 (29)	57 ± 15	
N5	20 – 22	355	0.03 ± 0.02 (0.05)	0.06 ± 0.06 (0.18)	4.2 ± 3.7 (11)	35 ± 7	0.0 ± 1.8

(24)	(21.3)	532	0.03 ± 0.01 (0.05)	0.06 ± 0.07 (0.19)	10 ± 11 (34)	63 ± 11	
N6 (25)	19 – 21 (19.3)	355	0.08 ± 0.01 (0.10)	0.09 ± 0.03 (0.16)	3.6 ± 0.8 (6.4)	46 ± 10	1.2 ± 0.6
		532	0.05 ± 0.01 (0.06)	0.06 ± 0.02 (0.11)	7.4 ± 1.8 (16)	65 ± 9	
N7 (26)	18 – 20 (19.1)	355	0.01 ± 0.01 (0.03)	0.02 ± 0.02 (0.06)	1.6 ± 0.5 (2.6)	44 ± 8	-
		532	-	-	2.7 ± 1.3 (5.3)	-	
N8 (27)	18 – 20 (19.1)	355	-	-	1.5 ± 0.1 (1.6)	-	-
		532	-	-	2.2 ± 0.1 (2.4)	-	

As expected following the time series of AEC profiles in Figure 1, the stratospheric AOD is extremely variable during the plume overpass. It ranges between almost four orders of magnitude with background values around 10^{-4} and maxima over 0.5 at both wavelengths. It is worth noting that the maximum of AOD is reached at 532 nm rather than at 355 nm as it is expected for most of the aerosol types. Such a result implies a negative Angström exponent (AE). AE are plotted with their corresponding LR at 355 nm in the scatterplot shown in Fig.3a. This graphic presentation highlights distinct aerosol clusters in the LR/AE plane. Taking into account the uncertainties on these values, only N6 stands out. We can still note a linear trend of the AE along time which is also corroborated by collocated atmospheric columnar properties issued by AERONET level 1.5 data (AERONET Link, 2022). Known to be inversely proportional to the particle size (Schuster et al., 2006), the lidar-derived AE indicate an aerosol size distribution driven by a coarse mode (N2 to N5) followed by a more typical value (1.2, N6) for ash free volcanic particles (Sellitto et al., 2017).

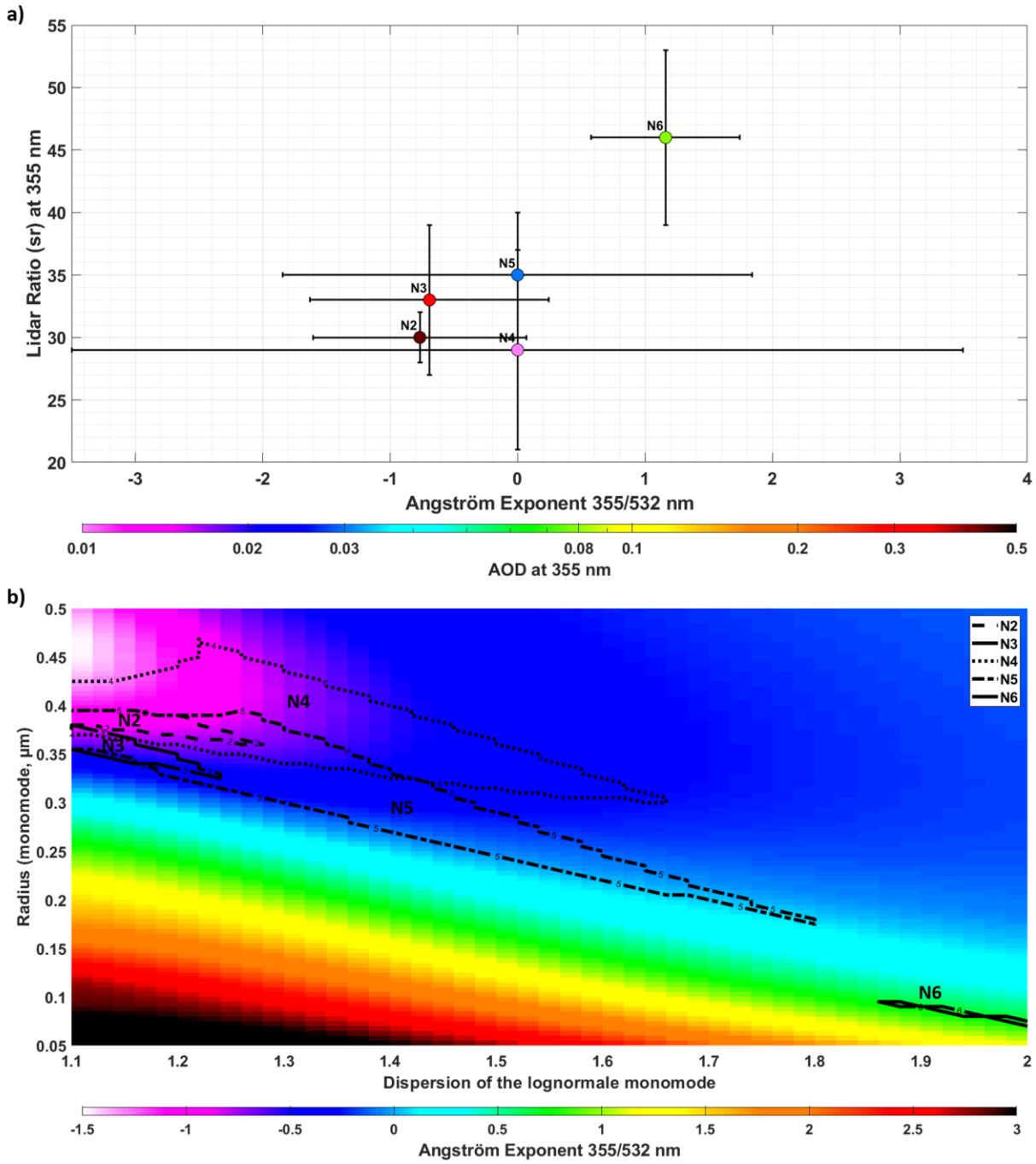

Figure 3: Scatterplot (a) of the Angström exponents and lidar ratio at 355 nm for N2 to N6. Lognormal monomode dispersion and corresponding particule radius cross-section of Angström exponent following Mie calculations for aerosol with sulfates properties (refractive index of 1.44 -5.10^{-3}i). The contours in (b) informs on the area in the dispersion/radius plane where the optical properties for N2 to N6 are in agreement with the Mie Scattering modeling. The contours constraints come from the uncertainties and standard deviations values given in Table1.

Negative values on AE are unusual, and to our knowledge, they have only been reported for coarse Saharan dust (e.g. Fernández et al., 2019; Rizzolo et al., 2017). To investigate these results we used a Mie code in order to reproduce such values. The hypothesis we made are : i) the presence

of spherical particles, which is justified for sulphates but less so if there is the presence of ash ; ii) a monomodal lognormal size distribution often reported by in situ measurements on stratospheric balloons and defined by its modal radius and dispersion (Chazette et al., 1995) and iii) an aerosol mixture with the properties of sulfates particles i.e. a real (imaginary) part of the refractive index of 1.44 (-5.10^{-3}). This hypothesis can be supported by the LR retrieved at 532 nm (~65 sr) which are coherent with the literature for volcanic aerosol driven by sulfates presence (Chazette et al., 1995 ; Prata et al., 2017). The AE is given in Fig. 3b against the modal radius and the dispersion of the lognormal size distribution. The same figure could be displayed for the LR at both 355 nm and 532 nm. The AE values matching with observations detailed in Table 1 are circled for the plumes from N2 to N6 where aerosol populations could exist under the previous hypothesies. One can notice that above a modal radius of 0.3 µm, a sulfates mixture may have a neagtive AE. We can conclude that if the VASL sampled above La Réunion comply with our hypothesis, the mean radius of the particle tend to decrease a little from ~0.4 to ~0.2 µm while the monomode get more and more dispersed, the dispersion increasing from ~1.1 to ~1.8. Finally the tail of the VSP (N6) could be composed of a fine mode aerosol fraction (radius around 0.1 µm) with large values of lognormal dispersion. Give the dispersion values of this VASL, N6 does probably not comply with the monomode hypothesis but could be a bimode lognormal distribution driven by the fine mode (considering the AE values above 1).

5 Discussion and summary

Lidar measurements performed over Reunion Island during the first passage of the stratospheric aerosol plume emanating from the HTHH volcano eruption show a plume structure marked by a very wide altitude range (18-36 km) along time. The highest aerosol layer is observed up to 36 km AMSL for the first time by ground-based lidars. This remarkably high altitude is linked to the impressive power inherent to this phreato-plinian eruption. Few days after the eruption, the altitude of the plume decrease with time over La Reunion. It is due to strong wind gradients in the stratosphere where the wind speed increased sharply with altitude. Radiosoundings performed from La Reunion highlighted a doubling of the zonal wind speed from 15 m s^{-1} at 20 km AMSL to 30 m s^{-1} at 30 km AMSL.

N1 presents surprising optical properties that could be inherent to this unprecedented eruption. In fact, the underwater caldera of the volcano and the power of the blast could have initially lift a complex mixing of aerosol that usually belong to the troposphere, including depolarizing particles such as ashes and/or sea salts. Yet, it is too delicate to conclude on this VASL based on just lidar measurements at 355 nm. However, the N2-N6 VASL turned out to be well sampled by both lidars. The synergy between these measurements allows to infer their optical properties in a more advanced way. First, we show that the AOD values recorded above La Réunion are, as far as we know, the highest ever recorded in the stratosphere (0.83 at 532 nm, peak SR of 403). According to the LR values, especially at 532 nm (~65 sr), and the known typical optical properties of volcanic aerosols, we expect to have observed a majority of sulfate particles. The unusually low AE values can be explained by the Mie theory following computation with monomode lognormal size distribution of sulfates particles with modal radius exceeding 0.3 µm in most of the cases (N2-N4). Our calculations show that these radius tend to decrease while the dispersion on the lognormal tend to increase. This result can be explained by two distinct processes. During a plinian eruption, the first injected particles are coarser than those that follow. Indeed, the atmosphere within the eruptive column is getting denser and denser as a lot of material is injected, it is then more and more difficult to lift corser and massive particles high in altitude (Brazier et al., 1983). This could

explaine the increasing tendency in the Angström exponent evolution along time and altitude. Furthermore, given the AE values of N2 and N3 (~-0.8) the size distribution of the particles must contain a significant coarse mode (Jarosławski et al., 2003) probably originating from hydrophilic growth and collisional processes occurring in dense and wet aerosol layers. Indeed, given the amount of water injected by this eruption, SO_2 conversion to sulfates and water uptake by these resulting particles could not be ignored (Kheykin et al, Submitted, Zhu et al., 2022).

To conclude, this study presents original observations of an exceptional volcanic event resulting in an unprecedented aerosol burden at these atltitude. Considering the lidar-derived optical aerosol properties, we can assess some microphysical properties of the volcanic aerosol layers. In a second step, it would be interesting to deepen these analysis considering the in situ measurements of water vapor, SO_2, and aerosols size distribution that have been made during some concomitant nights. This dataset could be an interesting challenge to converge to with microphysical aerosol modelling in chemistry transport models following such rare event. We then eventually be able to enhance our comprehension and modelisation capabilities of these complex stratospheric aerosol processes.

Aknowledgement

The authors acknowledge the Région Réunion, CNRS and Université de la Réunion for support and contribution within the research infrastructure OPAR (Observatoire de Physique de l'Atmosphère à la Réunion). OPAR is presently funded by CNRS (INSU), Météo France, and Université de la Réunion and managed by OSU-R (Observatoires des Sciences de l'Univers à la Réunion, UAR 3365). We also sincerely want to thank all the people for their contribution during the campaign to help with the measurements. By alphabetic order: Jean-Pierre Cammas, Eric Golubic, Yann Hello, Patrick Hernandez, Thierry Portafaix, Marion Ranaivombola. We also acknowledge the French Centre for Spatial Studies (CNES) for providing a research grant to the first author.

Data Availability Statement

The data used in this study are publicly accessible throught this webpage: https://geosur.osureunion.fr/geonetwork/srv/eng/catalog.search#/metadata/f2c35798-47b7-433c-8927-46cf7babca83.

References

AERONET Link. (2022). AERONET Lunar Aerosol Optical Depth Data Display Interface. Retrieved July 29, 2022, from https://aeronet.gsfc.nasa.gov/cgi-bin/data_display_aod_v3_lunar?site=Maido_OPAR&nachal=0&year=2022&month=1&aero_water=2&level=2&if_day=0&if_err=0&place_code=10&year_or_month=0

Amores, A., Monserrat, S., Marcos, M., Argüeso, D., Villalonga, J., Jordà, G., & Gomis, D. (2022). Numerical Simulation of Atmospheric Lamb Waves Generated by the 2022 Hunga-Tonga Volcanic Eruption. *Geophysical Research Letters*, *49*(6), e2022GL098240. https://doi.org/10.1029/2022GL098240

Angell, J. K. (1993). Comparison of stratospheric warming following Agung, El Chichon and Pinatubo volcanic eruptions. *Geophysical Research Letters*, *20*(8), 715–718. https://doi.org/10.1029/93GL00366

Angell, James K. (2000). Tropospheric temperature variations adjusted for El Niño, 1958–1998. *Journal of Geophysical Research: Atmospheres*, *105*(D9), 11841–11849. https://doi.org/10.1029/2000JD900044

Antuña, J. C., Robock, A., Stenchikov, G. L., Thomason, L. W., & Barnes, J. E. (2002). Lidar validation of SAGE II aerosol measurements after the 1991 Mount Pinatubo eruption. *Journal of Geophysical Research: Atmospheres*, *107*(D14), ACL 3-1-ACL 3-11. https://doi.org/10.1029/2001JD001441

Baray, J.-L., Courcoux, Y., Keckhut, P., Portafaix, T., Tulet, P., Cammas, J.-P., et al. (2013). Maïdo observatory: a new high-altitude station facility at Reunion Island (21° S, 55° E) for long-term atmospheric remote sensing and in situ measurements. *Atmospheric Measurement Techniques*, *6*(10), 2865–2877. https://doi.org/10.5194/amt-6-2865-2013

Bluth, G. J. S., Doiron, S. D., Schnetzler, C. C., Krueger, A. J., & Walter, L. S. (1992). Global tracking of the SO2 clouds from the June, 1991 Mount Pinatubo eruptions. *Geophysical Research Letters*, *19*(2), 151–154. https://doi.org/10.1029/91GL02792

Boville, B. A., Holton, J. R., & Mote, P. W. (1991). Simulation of the Pinatubo aerosol cloud in general circulation model. *Geophysical Research Letters*, *18*(12), 2281–2284. https://doi.org/10.1029/91GL02778

Brazier, S., Sparks, R. S. J., Carey, S. N., Sigurdsson, H., & Westgate, J. A. (1983). Bimodal grain size distribution and secondary thickening in air-fall ash layers. *Nature*, *301*(5896), 115–119. https://doi.org/10.1038/301115a0

CALIOP orbit N1, N. (2022). CALIOP orbit N1. Retrieved May 15, 2022, from https://www-calipso.larc.nasa.gov/products/lidar/browse_images/show_detail.php?s=expedited&v=V3-30&browse_date=2022-01-15&orbit_time=15-00-00&page=1&granule_name=CAL_LID_L1_Exp-Prov-V3-41.2022-01-15T15-00-00Z.hdf

Carr, J. L., Horváth, Á., Wu, D. L., & Friberg, M. D. (2022). Stereo Plume Height and Motion Retrievals for the Record-Setting Hunga Tonga-Hunga Ha'apai Eruption of 15 January 2022. *Geophysical Research Letters*, *49*(9), e2022GL098131. https://doi.org/10.1029/2022GL098131

Carvajal, M., Sepúlveda, I., Gubler, A., & Garreaud, R. (2022). Worldwide Signature of the 2022 Tonga Volcanic Tsunami. *Geophysical Research Letters*, *49*(6), e2022GL098153. https://doi.org/10.1029/2022GL098153

Chazette, P., David, C., Lefrère, J., Godin, S., Pelon, J., & Mégie, G. (1995). Comparative lidar study of the optical, geometrical, and dynamical properties of stratospheric post-volcanic aerosols, following the eruptions of El Chichon and Mount Pinatubo. *Journal of Geophysical Research: Atmospheres*, *100*(D11), 23195–23207. https://doi.org/10.1029/95JD02268

Chazette, Patrick, Bocquet, M., Royer, P., Winiarek, V., Raut, J.-C., Labazuy, P., et al. (2012). Eyjafjallajökull ash concentrations derived from both lidar and modeling. *Journal of Geophysical Research: Atmospheres*, *117*(D20). https://doi.org/10.1029/2011JD015755

DeFoor, T. E., Robinson, E., & Ryan, S. (1992). Early lidar observations of the June 1991 Pinatubo eruption plume at Mauna Loa Observatory, Hawaii. *Geophysical Research Letters*, *19*(2), 187–190. https://doi.org/10.1029/91GL02791

Delmas, R. J., Kirchner, S., Palais, J. M., & Petit, J.-R. (1992). 1000 years of explosive volcanism recorded at the South Pole. *Tellus B: Chemical and Physical Meteorology*, *44*(4), 335–350. https://doi.org/10.3402/tellusb.v44i4.15461

Dhomse, S. S., Mann, G. W., Antuña Marrero, J. C., Shallcross, S. E., Chipperfield, M. P., Carslaw, K. S., et al. (2020). Evaluating the simulated radiative forcings, aerosol properties, and stratospheric warmings from the 1963 Mt Agung, 1982 El Chichón, and 1991 Mt Pinatubo volcanic aerosol clouds. *Atmospheric Chemistry and Physics*, *20*(21), 13627–13654. https://doi.org/10.5194/acp-20-13627-2020

Di Virgilio, G., Evans, J. P., Blake, S. A. P., Armstrong, M., Dowdy, A. J., Sharples, J., & McRae, R. (2019). Climate Change Increases the Potential for Extreme Wildfires. *Geophysical Research Letters*, *46*(14), 8517–8526. https://doi.org/10.1029/2019GL083699

Dionisi, D., Keckhut, P., Courcoux, Y., Hauchecorne, A., Porteneuve, J., Baray, J. L., et al. (2015). Water vapor observations up to the lower stratosphere through the Raman lidar during the Maïdo Lidar Calibration Campaign. *Atmospheric Measurement Techniques*, *8*(3), 1425–1445. https://doi.org/10.5194/amt-8-1425-2015

Duflot, V., Baray, J.-L., Payen, G., Marquestaut, N., Posny, F., Metzger, J.-M., et al. (2017). Tropospheric ozone profiles by DIAL at Maïdo Observatory (Reunion Island): system description, instrumental performance and result comparison with ozone external data set. *Atmospheric Measurement Techniques*, *10*(9), 3359–3373. https://doi.org/10.5194/amt-10-3359-2017

Fernández, A. J., Sicard, M., Costa, M. J., Guerrero-Rascado, J. L., Gómez-Amo, J. L., Molero, F., et al. (2019). Extreme, wintertime Saharan dust intrusion in the Iberian Peninsula: Lidar monitoring and evaluation of dust forecast models during the February 2017 event. *Atmospheric Research*, *228*, 223–241. https://doi.org/10.1016/j.atmosres.2019.06.007

Gobbi, G. P., Congeduti, F., & Adriani, A. (1992). Early stratospheric effects of the Pinatubo Eruption. *Geophysical Research Letters*, *19*(10), 997–1000. https://doi.org/10.1029/92GL01038

Graft, H.-F., Kirchner, I., Robock, A., & Schult, I. (1993). Pinatubo eruption winter climate effects: model versus observations. *Climate Dynamics*, *9*(2), 81–93. https://doi.org/10.1007/BF00210011

Grant, W. B., Fishman, J., Browell, E. V., Brackett, V. G., Nganga, D., Minga, A., et al. (1992). Observations of reduced ozone concentrations in the tropical stratosphere after the eruption of Mt. Pinatubo. *Geophysical Research Letters*, *19*(11), 1109–1112. https://doi.org/10.1029/92GL01153

Guo, S., Bluth, G. J. S., Rose, W. I., Watson, I. M., & Prata, A. J. (2004). Re-evaluation of SO2 release of the 15 June 1991 Pinatubo eruption using ultraviolet and infrared satellite sensors. *Geochemistry, Geophysics, Geosystems*, *5*(4). https://doi.org/10.1029/2003GC000654

Hansen, J., Lacis, A., Ruedy, R., & Sato, M. (1992). Potential climate impact of Mount Pinatubo eruption. *Geophysical Research Letters*, *19*(2), 215–218. https://doi.org/10.1029/91GL02788

Hersbach, H., Bell, B., Berrisford, P., Hirahara, S., Horányi, A., Muñoz-Sabater, J., et al. (2020). The ERA5 global reanalysis. *Quarterly Journal of the Royal Meteorological Society*, *146*(730), 1999–2049. https://doi.org/10.1002/qj.3803

Jarosławski, J., Krzyścin, J. W., Puchalski, S., & Sobolewski, P. (2003). On the optical thickness in the UV range: Analysis of the ground-based data taken at Belsk, Poland. *Journal of Geophysical Research: Atmospheres*, *108*(D23). https://doi.org/10.1029/2003JD003571

Khaykin, S., Legras, B., Bucci, S., Sellitto, P., Isaksen, L., Tencé, F., et al. (2020). The 2019/20 Australian wildfires generated a persistent smoke-charged vortex rising up to 35 km altitude. *Communications Earth & Environment*, *1*(1), 1–12. https://doi.org/10.1038/s43247-020-00022-5

Khaykin, S., Podglajen, A., Ploeger, F., Grooß, J.-U., Tencé, F., Bekki, S., et al. (Submitted). Global perturbation of stratospheric water and aerosol burden by Hunga eruption. *Communications Earth & Environment*.

Klett, J. D. (1985). Lidar inversion with variable backscatter/extinction ratios. *Applied Optics*, *24*(11), 1638–1643. https://doi.org/10.1364/AO.24.001638

Kremser, S., Thomason, L. W., von Hobe, M., Hermann, M., Deshler, T., Timmreck, C., et al. (2016). Stratospheric aerosol—Observations, processes, and impact on climate. *Reviews of Geophysics*, *54*(2), 278–335. https://doi.org/10.1002/2015RG000511

Legras, B., Duchamp, C., Sellitto, P., Podglajen, A., Carboni, E., Siddans, R., et al. (2022). The evolution and dynamics of the Hunga Tonga plume in the stratosphere. *EGUsphere*, 1–19. https://doi.org/10.5194/egusphere-2022-517

McCormick, M. P., & Veiga, R. E. (1992). SAGE II measurements of early Pinatubo aerosols. *Geophysical Research Letters*, *19*(2), 155–158. https://doi.org/10.1029/91GL02790

McCormick, M. Patrick, Thomason, L. W., & Trepte, C. R. (1995). Atmospheric effects of the Mt Pinatubo eruption. *Nature*, *373*(6513), 399–404. https://doi.org/10.1038/373399a0

Millán, L., Santee, M. L., Lambert, A., Livesey, N. J., Werner, F., Schwartz, M. J., et al. (2022). The Hunga Tonga-Hunga Ha'apai Hydration of the Stratosphere. *Geophysical Research Letters*, *49*(13), e2022GL099381. https://doi.org/10.1029/2022GL099381

Minnis, P., Harrison, E. F., Stowe, L. L., Gibson, G. G., Denn, F. M., Doelling, D. R., & Smith, W. L. (1993). Radiative Climate Forcing by the Mount Pinatubo Eruption. *Science*, *259*(5100), 1411–1415. https://doi.org/10.1126/science.259.5100.1411

Müller, D., Ansmann, A., Mattis, I., Tesche, M., Wandinger, U., Althausen, D., & Pisani, G. (2007). Aerosol-type-dependent lidar ratios observed with Raman lidar. *Journal of Geophysical Research*, *112*(D16), D16202. https://doi.org/10.1029/2006JD008292

Peterson, D. A., Campbell, J. R., Hyer, E. J., Fromm, M. D., Kablick, G. P., Cossuth, J. H., & DeLand, M. T. (2018). Wildfire-driven thunderstorms cause a volcano-like stratospheric injection of smoke. *Npj Climate and Atmospheric Science*, *1*(1), 1–8. https://doi.org/10.1038/s41612-018-0039-3

Pierangelo, C., Chédin, A., & Chazette, P. (2004). Measurements of stratospheric volcanic aerosol optical depth from NOAA TIROS Observational Vertical Sounder (TOVS) observations: VOLCANIC AEROSOL FROM NOAA/TOVS. *Journal of Geophysical Research: Atmospheres*, *109*(D3), n/a-n/a. https://doi.org/10.1029/2003JD003870

Poli, P., & Shapiro, N. M. (2022). Rapid Characterization of Large Volcanic Eruptions: Measuring the Impulse of the Hunga Tonga Ha'apai Explosion From Teleseismic Waves. *Geophysical Research Letters*, *49*(8), e2022GL098123. https://doi.org/10.1029/2022GL098123

Prata, A. T., Young, S. A., Siems, S. T., & Manton, M. J. (2017). Lidar ratios of stratospheric volcanic ash and sulfate aerosols retrieved from CALIOP measurements. *Atmospheric Chemistry and Physics*, *17*(13), 8599–8618. https://doi.org/10.5194/acp-17-8599-2017

Rizzolo, J. A., Barbosa, C. G. G., Borillo, G. C., Godoi, A. F. L., Souza, R. A. F., Andreoli, R. V., et al. (2017). Soluble iron nutrients in Saharan dust over the central Amazon rainforest. *Atmospheric Chemistry and Physics*, *17*(4), 2673–2687. https://doi.org/10.5194/acp-17-2673-2017

Robock, A. (2015). Chapter 53 - Climatic Impacts of Volcanic Eruptions. In H. Sigurdsson (Ed.), *The Encyclopedia of Volcanoes (Second Edition)* (pp. 935–942). Amsterdam: Academic Press. https://doi.org/10.1016/B978-0-12-385938-9.00053-5

Robock, A., & Mao, J. (1995). The Volcanic Signal in Surface Temperature Observations. *Journal of Climate*, *8*(5), 1086–1103. https://doi.org/10.1175/1520-0442(1995)008<1086:TVSIST>2.0.CO;2

Schuster, G. L., Dubovik, O., & Holben, B. N. (2006). Angstrom exponent and bimodal aerosol size distributions. *Journal of Geophysical Research: Atmospheres*, *111*(D7). https://doi.org/10.1029/2005JD006328

Sellitto, P., Salerno, G., La Spina, A., Caltabiano, T., Terray, L., Gauthier, P.-J., & Briole, P. (2017). A novel methodology to determine volcanic aerosols optical properties in the UV and NIR and Ångström parameters using Sun photometry. *Journal of Geophysical Research: Atmospheres*, *122*(18), 9803–9815. https://doi.org/10.1002/2017JD026723

Tejedor, E., Steiger, N., Smerdon, J. E., Serrano-Notivoli, R., & Vuille, M. (2021). Global Temperature Responses to Large Tropical Volcanic Eruptions in Paleo Data Assimilation Products and Climate Model Simulations Over the Last Millennium. *Paleoceanography and Paleoclimatology*, *36*(4), e2020PA004128. https://doi.org/10.1029/2020PA004128

Vérèmes, H., Payen, G., Keckhut, P., Duflot, V., Baray, J.-L., Cammas, J.-P., et al. (2019). Validation of the Water Vapor Profiles of the Raman Lidar at the Maïdo Observatory (Reunion Island) Calibrated with Global Navigation Satellite System Integrated Water Vapor. *Atmosphere*, *10*(11), 713. https://doi.org/10.3390/atmos10110713

Vergoz, J., Hupe, P., Listowski, C., Le Pichon, A., Garcés, M. A., Marchetti, E., et al. (2022). IMS observations of infrasound and acoustic-gravity waves produced by the January 2022 volcanic eruption of Hunga, Tonga: A global analysis. *Earth and Planetary Science Letters*, *591*, 117639. https://doi.org/10.1016/j.epsl.2022.117639

Vernier, J.-P., Thomason, L. W., Pommereau, J.-P., Bourassa, A., Pelon, J., Garnier, A., et al. (2011). Major influence of tropical volcanic eruptions on the stratospheric aerosol layer during the last decade. *Geophysical Research Letters*, *38*(12). https://doi.org/10.1029/2011GL047563

Winker, D. M., Pelon, J. R., & McCormick, M. P. (2003). The CALIPSO mission: spaceborne lidar for observation of aerosols and clouds. In U. N. Singh, T. Itabe, & Z. Liu (Eds.) (p. 1). Presented at the Third International Asia-Pacific Environmental Remote Sensing Remote Sensing of the Atmosphere, Ocean, Environment, and Space, Hangzhou, China. https://doi.org/10.1117/12.466539

Yu, P., Toon, O. B., Bardeen, C. G., Zhu, Y., Rosenlof, K. H., Portmann, R. W., et al. (2019). Black carbon lofts wildfire smoke high into the stratosphere to form a persistent plume. *Science*. https://doi.org/10.1126/science.aax1748

Yuen, D. A., Scruggs, M. A., Spera, F. J., Zheng, Y., Hu, H., McNutt, S. R., et al. (2022). Under the surface: Pressure-induced planetary-scale waves, volcanic lightning, and gaseous clouds caused by the submarine eruption of Hunga Tonga-Hunga Ha'apai volcano. *Earthquake Research Advances*, 100134. https://doi.org/10.1016/j.eqrea.2022.100134

Zhu, Y., Bardeen, C., Tilmes, S., Mills, M., Harvey, V., Taha, G., et al. (2022). *2022 Hunga-Tonga eruption: stratospheric aerosol evolution in a water-rich plume* (preprint). In Review. https://doi.org/10.21203/rs.3.rs-1647643/v1